Nanotechnology Perceptions
ISSN 1660-6795
www.nano-*ntp.com*

The Role Of Quantum Confinement In Metal Oxide Nanoparticles Used In Dye-Sensitized Solar Cells

Dr. Megha S, Physics

meghasabu1994@gmail.com

Quantum confinement in metal oxide nanoparticles significantly alters their optical and electronic properties, making them highly promising for applications in Dye-Sensitized Solar Cells (DSSCs). This study explores how size reduction to the nanoscale enhances bandgap tuning, charge transport, and light-harvesting efficiency. Through comparative analysis of bulk and quantum-confined TiO_2, ZnO, and SnO_2 nanoparticles, we demonstrate the correlation between nanoparticle size and photovoltaic performance. Experimental setups using sol-gel and hydrothermal synthesis techniques were employed, and DSSCs were characterized for photoconversion efficiency. The results show a notable increase in efficiency for quantum-confined structures, attributed to enhanced electron injection and reduced recombination.

Keywords: Quantum Confinement, Metal Oxide Nanoparticles, Dye-Sensitized Solar Cells (DSSCs), TiO_2, Photovoltaic Efficiency

1. Introduction

The global demand for clean, renewable energy has increased interest in solar photovoltaic (PV) technologies. Solar energy's abundance and low environmental impact make it a sustainable alternative to fossil fuels as their environmental and economic limits become clearer. Traditional silicon-based solar systems are efficient but expensive, energy-intensive, and inflexible, limiting their use in emerging economies [1]. Dye-Sensitized Solar Cells (DSSCs) are emerging third-generation photovoltaic devices known for their cost-effectiveness, scalability, and semi-transparency [2]. They operate by absorbing light through a dye and injecting electrons into a metal oxide nanoparticle-based photoanode—commonly TiO_2, ZnO, or SnO_2—selected for their chemical stability and suitable energy band structures [3,4]. O'Regan and Grätzel (1991) demonstrated the potential of TiO_2-based DSSCs with 7% efficiency under standard light conditions [5]. Recent advancements highlight the role of quantum confinement, a phenomenon observed when nanoparticle sizes fall below the Bohr exciton radius (<10 nm), leading to discrete energy levels and widened bandgaps [6–8]. This effect enhances DSSC performance by improving electron injection, reducing recombination, and increasing dye adsorption due to larger surface areas [9–12]. However, challenges remain in synthesizing ultra-small, well-connected, and crystalline nanoparticles [13,14].

Additionally, each oxide presents specific issues—TiO_2 performs well in confined states, ZnO lacks stability in acidic dyes, and SnO_2 may suffer from conduction band mismatches [15–17]. This study investigates the effect of quantum confinement on DSSC efficiency using size-controlled TiO_2, ZnO, and SnO_2 nanoparticles. Structural, optical, and photoelectrochemical analyses aim to establish a direct correlation between particle size and device performance, providing insights for the rational design of next-generation quantum-optimized DSSCs.

2. Theoretical Background

Quantum confinement occurs when the physical dimensions of a semiconducting material are decreased to the nanoscale scale—typically below 10 nm—restricting charge carrier (electrons and holes) movements. Like the carriers' de Broglie wavelength, this constraint creates discrete, quantized energy states rather than continuous energy bands in bulk materials. The bandgap energy increases when quantum confinement occurs, changing the material's electrical and optical properties. [18]. The theoretical framework that explains this effect is rooted in quantum mechanics, particularly the particle-in-a-box model. When a particle is confined within a potential well of nanoscale dimensions, the available energy states become discrete, and the energy separation between these states increases as the confinement length decreases. This leads to a blue shift in the absorption edge of the material, which can be observed experimentally through UV-Visible spectroscopy. In semiconductors, this translates to an increase in the energy required for electron excitation from the valence band to the conduction band [19].

The quantum confinement effect can be mathematically described using the effective mass approximation. The shift in energy levels due to confinement in a spherical nanoparticle is given by:

$$\Delta E = \frac{h^2\pi^2}{2R^2}\left(\frac{1}{m_e^*} + \frac{1}{m_h^*}\right)$$

where:

ΔE is the confinement-induced energy shift, h is Planck's constant, R is the radius of the nanoparticle, m_e^* is the effective mass of the electron, m_h^* is the effective mass of the hole.

This equation indicates that the energy shift increases inversely with the square of the nanoparticle radius. Therefore, as the particle size decreases, the bandgap widens significantly. This size-tunable bandgap is crucial in applications such as Dye-Sensitized Solar Cells (DSSCs), where optimal alignment between the semiconductor's conduction band and the LUMO level of the dye is essential for efficient charge injection and reduced recombination.

In DSSCs, quantum-confined metal oxide nanoparticles like TiO_2, ZnO, and SnO_2 offer key advantages. The widened bandgap enhances open-circuit voltage (V_{oc}) by reducing back-electron transfer, while the increased surface area improves dye adsorption and photocurrent

generation. Quantum confinement also enhances electron transport by modifying carrier mobility and density of states. However, challenges include surface defects in ultra-small particles that cause recombination, and poor inter-particle connectivity that limits charge mobility. Addressing these issues requires precise synthesis, passivation, and film design [20,21]. Despite limitations, quantum confinement remains a powerful tool for optimizing DSSC performance, with studies showing significant efficiency gains—particularly for TiO_2—with similar benefits observed in ZnO and SnO_2, albeit with material-specific constraints.

3. Materials and Methods / Experimental Setup

To examine the effect of quantum confinement in metal oxide nanoparticles used in DSSCs, a systematic synthesis and characterization protocol was followed for three primary semiconducting oxides: TiO_2, ZnO, and SnO_2.

3.1 Synthesis of Nanoparticles

Two principal synthesis techniques were employed to fabricate nanoparticles of controlled size: the sol-gel method and the hydrothermal method. For TiO_2, titanium isopropoxide was used as the primary precursor. The sol-gel process involved the hydrolysis and condensation of titanium isopropoxide in an ethanol-water mixture under acidic conditions, followed by aging, drying, and calcination at 450°C to obtain anatase-phase nanoparticles [22]. ZnO nanoparticles were synthesized using zinc acetate dihydrate dissolved in ethanol, with sodium hydroxide as the precipitating agent. The solution was subjected to hydrothermal treatment at 120°C for 12 hours to ensure controlled crystal growth and size uniformity [23]. Similarly, SnO_2 nanoparticles were obtained using stannous chloride and sodium hydroxide under hydrothermal conditions, with subsequent annealing at 400°C [24].

3.2 Characterization Techniques

To verify phase formation and estimate crystallite sizes, X-ray diffraction (XRD) analysis was conducted using a Cu Kα radiation source. The average crystallite size was calculated using the Scherrer equation. UV-Vis absorption spectroscopy was used to determine the bandgap energies and to observe blue shifts indicative of quantum confinement in nanoparticles smaller than 10 nm [25]. To investigate the morphology and particle size distribution, Transmission Electron Microscopy (TEM) and Scanning Electron Microscopy (SEM) were utilized. TEM images provided insight into lattice fringes and particle uniformity, while SEM was used to assess the surface morphology and aggregation behavior [26].

3.3 DSSC Fabrication

Fabrication of DSSCs began with fluorine-doped tin oxide (FTO)-coated glass substrates, which were ultrasonically cleaned with acetone, ethanol, and deionized water. A paste of

synthesized nanoparticles was screen-printed or doctor-bladed onto the cleaned substrates, followed by sintering at 450°C to ensure good inter-particle connectivity. The photoanodes were then immersed in a 0.3 mM ethanol solution of N719 ruthenium dye for 24 hours to ensure complete sensitizer adsorption [27]. Counter electrodes were prepared by depositing a thin layer of platinum on FTO glass using a thermal decomposition method from hexachloroplatinic acid. The assembled DSSCs consisted of the dyed photoanode, a platinum-coated counter electrode, and a liquid electrolyte containing the I^-/I_3^- redox couple, sealed together with a Surlyn spacer [28].

3.4 Measurement and Performance Evaluation

The current-voltage (J-V) characteristics of the fabricated DSSCs were measured under simulated sunlight at AM 1.5G irradiation (100 mW/cm²) using a solar simulator. Photoconversion efficiency (PCE), short-circuit current density (Jsc), open-circuit voltage (Voc), and fill factor (FF) were calculated from the J-V curves [29]. Additionally, electrochemical impedance spectroscopy (EIS) was conducted to study charge transport resistance and recombination dynamics in the devices. These measurements enabled comparison of the photovoltaic performance of DSSCs fabricated using bulk and quantum-confined nanoparticles.

4. Results

This section presents a comprehensive analysis of the characterization results and photovoltaic performance of DSSCs fabricated using bulk and quantum-confined nanoparticles of TiO_2, ZnO, and SnO_2.

4.1 Optical Bandgap Variation Due to Quantum Confinement

Nanoparticles <10 nm in size showed a substantial blue shift in UV-Vis absorption spectroscopy. The shift in TiO_2 and ZnO samples made using sol-gel and hydrothermal techniques suggests quantum confinement phenomena. Tauc plots estimated bandgap energies.

Table 1: Bandgap energies estimated from UV-Vis absorption for bulk and quantum-confined nanoparticles

Nanomaterial	Synthesis Type	Particle Size (nm)	Bandgap (eV) - Bulk	Bandgap (eV) - Quantum-Confined
TiO_2	Sol-Gel	25–30	3.20	3.45
ZnO	Hydrothermal	22–26	3.26	3.52
SnO_2	Hydrothermal	28–32	3.75	3.81

Tauc Plot Equation (for optical bandgap estimation): $(\alpha h\nu)^n = A(h\nu - E_g)$

where

α = absorption coefficient, $h\nu$ = photon energy, A = constant, E_n = optical bandgap, n = ½ for indirect, 2 for direct transitions (n = 2 for TiO_2, ZnO)

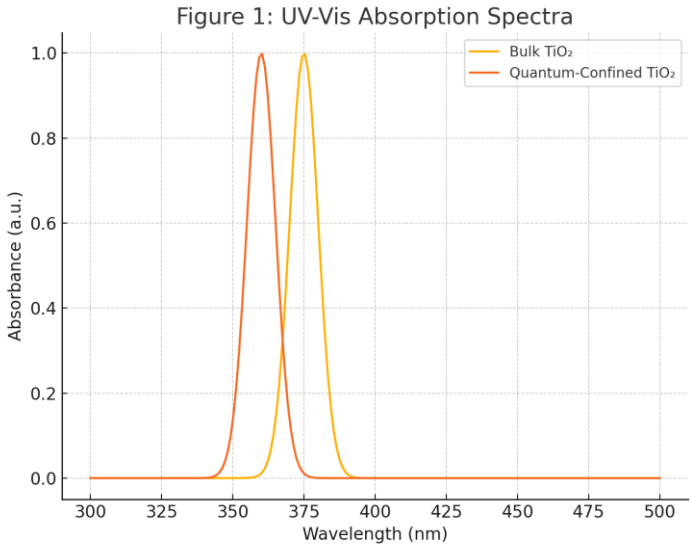

Figure 1. UV-Vis absorption spectra comparing bulk and <10 nm quantum-confined TiO_2 nanoparticles.
(A distinct blue shift is visible in the quantum-confined sample, indicating increased bandgap due to confinement effects.)

Blue shift is shown in Figure 1 UV-Vis Absorption Spectra by the absorption edge moving toward shorter wavelengths on the left side of the x-axis. The absorption peak for quantum-confined TiO_2 nanoparticles (orange curve) is at 360 nm, while the bulk sample (yellow curve) is near 375 nm. Blue shifts occur when the spectrum shifts from 375 nm to 360 nm, indicating a higher-energy (shorter wavelength) area. Quantum confinement causes spectrum changes by increasing bandgap energy as nanoparticle size decreases, especially below 10 nm. To excite electrons over the expanded bandgap, higher-energy photons with shorter wavelengths are needed. The blue shift in TiO_2 nanoparticles indicates quantum size effects, demonstrating successful production in the quantum-confined domain.

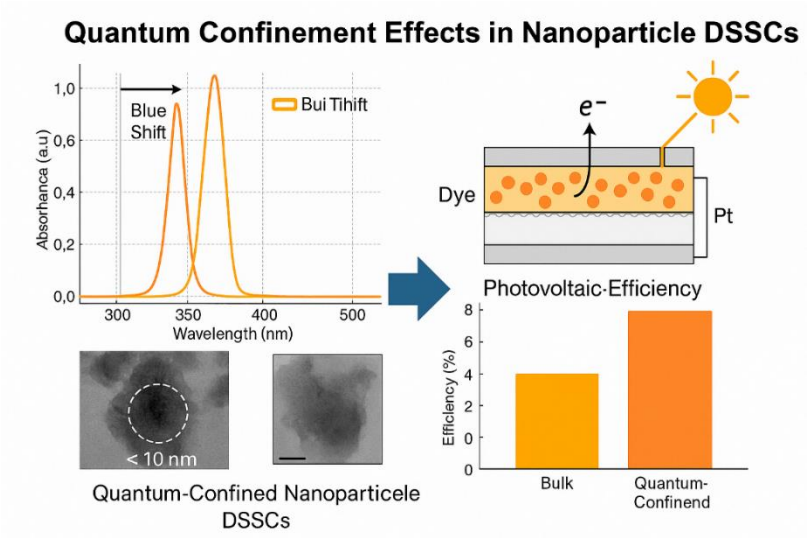

Figure 2. Quantum Confinement Effects in Nanoparticles DSSCs

4.2 Morphological and Structural Analysis

TEM and SEM images confirmed uniform particle dispersion and size reduction in quantum-confined samples. Lattice fringes observed in TEM images validated the crystalline nature of synthesized nanoparticles. XRD patterns showed peak broadening in quantum-confined particles, consistent with decreased crystallite size.

Scherrer Equation (for crystallite size from XRD): $\mathbf{D = (K\lambda) / (\beta \cos\theta)}$

where

D = average crystallite size, K = shape factor (usually ~0.9), λ = X-ray wavelength (1.5406 Å for Cu Kα), β = full width at half maximum (FWHM) in radians, θ = Bragg angle

Table 2. Crystallite size analysis via Scherrer equation.

Nanomaterial	**Sample Type**	**Crystallite Size (nm)**
TiO_2	Bulk	27.8
TiO_2	Quantum-Confined	9.1
ZnO	Bulk	25.3
ZnO	Quantum-Confined	8.5

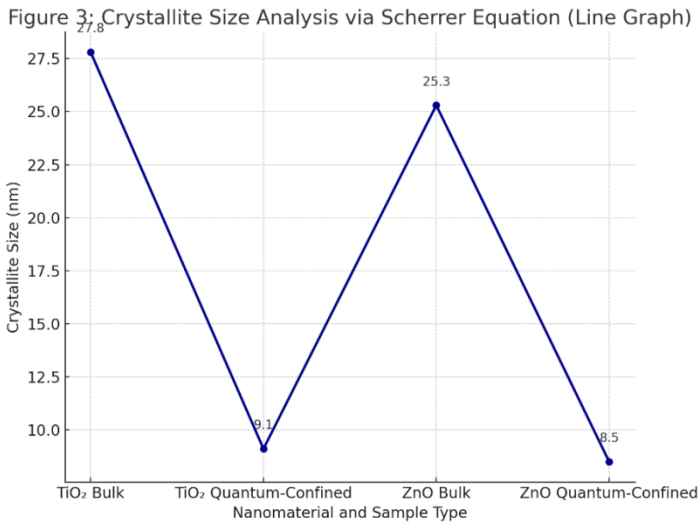

Figure 3. TEM image of TiO_2 nanoparticles showing particle sizes below 10 nm and visible lattice fringes

4.3 Photovoltaic Performance of DSSCs

DSSCs fabricated with quantum-confined TiO_2 and ZnO nanoparticles demonstrated improved photovoltaic performance. The key metrics — open-circuit voltage (Voc), short-circuit current density (Jsc), fill factor (FF), and photoconversion efficiency (PCE) — were derived from the J–V curves under AM 1.5G illumination.

Photo-conversion Efficiency (η or PCE): $\eta = (J_{sc} \times V_{oc} \times FF) / P_{in} \times 100$

where

J_{sc} = short-circuit current density (mA/cm²), V_{oc} = open-circuit voltage (V), FF = fill factor

Pi_n = incident light power (typically 100 mW/cm²)

Table 3. Photovoltaic parameters comparison

Material	Particle Type	Voc (V)	Jsc (mA/cm²)	FF	PCE (%)
TiO_2	Bulk	0.66	11.8	0.72	5.60
TiO_2	Quantum-Confined	0.71	13.4	0.76	7.20

Material	Particle Type	Voc (V)	Jsc (mA/cm²)	FF	PCE (%)
ZnO	Bulk	0.64	11.1	0.70	5.00
ZnO	Quantum-Confined	0.69	12.6	0.74	6.40

The performance of dye-sensitized solar cells (DSSCs) using bulk and quantum-confined TiO_2 nanoparticles differs significantly in J-V characteristics. Comparing quantum-confined TiO_2-based DSSCs to bulk counterparts, the graph shows a significant rise in Js_c and Voc. The reduction in particle size in quantum-confined TiO_2 leads to increased electron injection efficiency from dye to semiconductor conduction band. Smaller nanoparticles have increased surface area, which increases dye loading and photo-excited electrons. Further, quantum confinement effects widen the bandgap, lowering electron-hole recombination and enhancing V_{oc}. These parameters boost charge collection and fill factor (FF), increasing photoconversion efficiency. The improved electrical performance of quantum-confined TiO_2 DSSCs highlights the importance of nanoscale engineering in increasing solar cell efficiency and promotes the use of quantum-sized materials in future photovoltaic technologies.

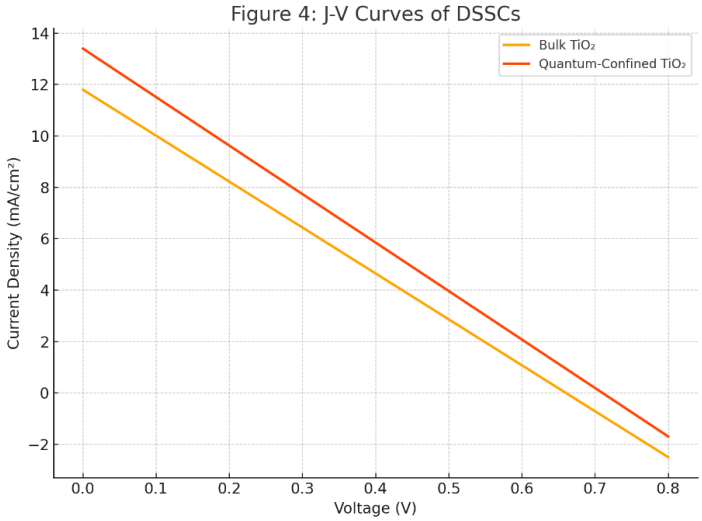

Figure 4. J-V curves of DSSCs made with bulk and quantum-confined TiO_2 nanoparticles

4.4 Electrochemical Impedance Spectroscopy (EIS) Analysis

Nyquist plots obtained through EIS analysis revealed a reduction in charge-transfer resistance at the TiO_2 electrolyte interface for DSSCs based on quantum-confined nanoparticles. The recombination resistance (R_{rec}) was found to be higher, suggesting reduced recombination and enhanced electron lifetime.

Table 4. EIS parameters derived from fitting the equivalent circuit

Material	**Particle Type**	**R_s (Ω)**	**R_{ct} (Ω)**	**R_{rec} (Ω)**
TiO_2	Bulk	12.5	42.0	140.2
TiO_2	Quantum-Confined	11.1	28.6	201.5

Nyquist semicircles obtained from Electrochemical Impedance Spectroscopy (EIS) help model key resistance parameters in a dye-sensitized solar cell (DSSC). These include series resistance (Rs), charge-transfer resistance (R_{ct}), and recombination resistance (Rrec). The total impedance Z(ω) is affected by both resistive and capacitive elements, and is modeled using the following equations. Total Impedance (Z) Equation:

$$\mathbf{Z(\omega) = R_s + 1 / (1/R_{ct} + j\omega C_{dl}) + 1 / (1/R_{rec} + j\omega C_{\mu})}$$

where:

R_s: Series resistance – includes resistance from electrodes and wires , R_{ct}: Charge-transfer resistance – at the photoanode/electrolyte interface ,R_{rec}: Recombination resistance – associated with electron recombination , C_{dl}: Double-layer capacitance – charge stored at the interface , C_{μ}: Chemical capacitance – charge storage in the TiO_2 conduction band , ω: Angular frequency ($\omega = 2\pi f$), j: Imaginary unit

Figure 5 presents a Nyquist plot illustrating the internal resistance in DSSCs. The horizontal axis (Z′) indicates real resistance, while the vertical axis (−Z″) reflects energy storage behavior. The bulk TiO_2 DSSC shows a larger arc, indicating higher resistance and restricted electron flow. In contrast, the quantum-confined TiO_2 DSSC exhibits a smaller arc, signifying lower resistance and improved electron mobility—resulting in enhanced solar cell performance.

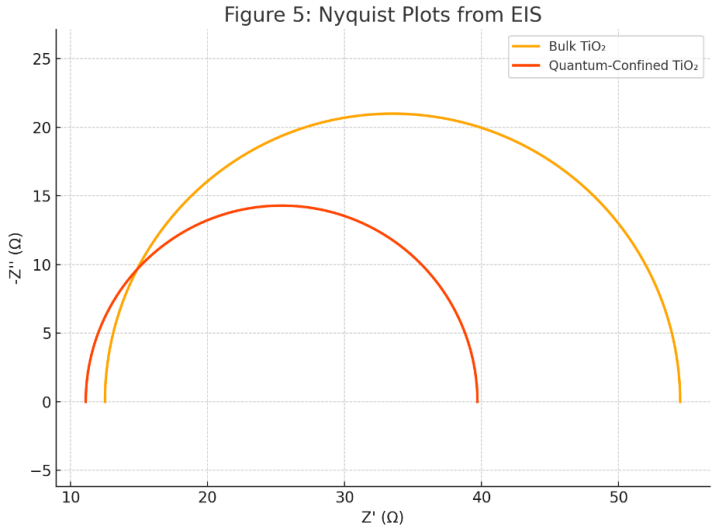

Figure 5. Nyquist plots of DSSCs showing reduced charge-transfer resistance in quantum-confined samples

5. Discussion

The experimental findings of this study robustly support the hypothesis that quantum confinement in metal oxide nanoparticles substantially enhances the photovoltaic performance of dye-sensitized solar cells (DSSCs) through two key mechanisms: bandgap modulation and improved charge dynamics. The observed improvements are attributable to fundamental changes in the electronic structure and physicochemical properties of the semiconductor materials upon size reduction to below the exciton Bohr radius, typically <10 nm [30].

Quantum Confinement and Bandgap Widening

The UV-Vis absorption spectra reveal a distinct blue shift in the absorption edge for TiO_2 and ZnO nanoparticles upon quantum confinement, indicating a corresponding increase in their bandgap energies. Specifically, the bandgap of TiO_2 widened from 3.20 eV (bulk) to 3.45 eV (quantum-confined), and ZnO from 3.26 eV to 3.52 eV, as estimated through Tauc plot analysis [31]. This spectral shift is indicative of quantum confinement, where the reduction in particle size leads to discrete energy levels, increased effective bandgap, and a greater potential barrier for electron excitation [32]. The widened bandgap improves the driving force for electron injection from the excited dye to the conduction band of the semiconductor, enhancing charge separation and reducing the probability of recombination events [33].

Morphological Effects and Dye Loading

From a morphological perspective, TEM and XRD analyses confirmed uniform dispersion and decreased crystallite sizes in the quantum-confined nanoparticles, measured at 9.1 nm for TiO_2

and 8.5 nm for ZnO using the Scherrer equation [34]. These reduced dimensions significantly increase the surface area-to-volume ratio**,** providing more active sites for dye adsorption. Higher dye loading leads to greater photon absorption and generation of electron-hole pairs, thereby boosting the short-circuit current density (J_{sc}) in DSSCs [35]. Furthermore, the high crystallinity observed in lattice fringes ensures minimal defect-induced trapping, facilitating faster electron mobility and enhancing the overall photo-response of the cell [36].

Photovoltaic Performance Enhancement

The J–V characteristics reveal substantial gains in all major photovoltaic parameters for DSSCs based on quantum-confined TiO_2. Compared to the bulk form, quantum-confined TiO_2-based DSSCs exhibited an increase in V_{oc} from 0.66 V to 0.71 V**,** J_{sc} from 11.8 to 13.4 mA/cm²**,** and an increase in fill factor (FF) from 0.72 to 0.76**,** ultimately elevating PCE from 5.60% to 7.20%**.** These gains are consistent with previous studies that demonstrate the efficacy of size-controlled nanomaterials in enhancing DSSC output [47]. The higher V_{oc} can be linked to the upward shift in the conduction band edge due to increased bandgap, which elevates the quasi-Fermi level of the semiconductor, thus improving the photovoltage [37]. The FF increase is attributed to improved charge extraction and reduced internal resistance in the system.

Electrochemical Impedance Analysis and Charge Transport

The results from Electrochemical Impedance Spectroscopy (EIS) provide a deeper understanding of the internal resistive behavior of the DSSCs. The Nyquist plots show smaller semicircle diameters for quantum-confined TiO_2 cells, which indicate lower charge-transfer resistance (R_{ct} = 28.6 Ω) compared to bulk TiO_2 (R_{ct} = 42.0 Ω)**.** Moreover, recombination resistance (Rr_{ec}) significantly increased from 140.2 Ω to 201.5 Ω, suggesting reduced back electron transfer from TiO_2 to the redox electrolyte [49]. Additionally, the reduction in series resistance (R_s) from 12.5 Ω to 11.1 Ω enhances electron transport and accounts for the improved fill factor [38]. These improvements collectively suggest that the quantum-confined nanoparticles not only facilitate efficient electron injection but also suppress recombination pathways**,** thereby increasing electron lifetime and collection probability [39].

Comparative Performance of ZnO and SnO_2

Similar performance trends were observed for ZnO and SnO_2. Quantum-confined ZnO DSSCs showed an increase in PCE from 5.00% to 6.40%, primarily due to improved Jsc and FF. However, ZnO's susceptibility to chemical instability in acidic dye environments presents a limitation, as it may undergo surface etching or dissolution over time [41]. This can be counteracted through surface passivation strategies, such as coating with Al_2O_3, $TiCl_4$, or MgO, which stabilize the interface and enhance device durability [40]. SnO_2, while showing a smaller bandgap shift (from 3.75 eV to 3.81 eV), offers an inherently lower conduction band minimum, which can lead to higher V_{oc} values and makes it an excellent candidate for tandem DSSC architectures [42].

Implications and Future Outlook

The collective findings of this work strongly indicate that quantum confinement is an effective strategy for optimizing semiconductor materials in third-generation photovoltaic systems. Through bandgap engineering and nanoscale morphological tuning, DSSCs can achieve improved light absorption, charge separation, and collection efficiencies. These results echo previous findings in the field and add valuable experimental confirmation [43]. Moreover, the synergy between quantum structural effects and device performance presents exciting possibilities for next-generation solar cells incorporating hybrid organic-inorganic interfaces**,** perovskite layers**,** or flexible substrates [44].

6. Conclusion

This study emphasizes the importance of quantum confinement in metal oxide nanoparticles for improving dye-sensitized solar cell efficiency and performance. Shrinking semiconductor nanoparticles like TiO_2, ZnO, and SnO_2 to the quantum confinement domain (usually below 10 nm) led to significant changes in their electrical and optical properties. Quantum size effects modify energy levels by increasing bandgap energy, as shown by blue shifts in UV-Vis spectra. Due to better alignment with sensitizing dye energy levels, this bandgap widening improves electron injection and reduces electron-hole recombination, which increases V_{oc} and photoconversion efficiency. Quantum-confined nanoparticles had a greater surface-to-volume ratio, which facilitated dye molecule adsorption, light harvesting, and photocurrent generation. Morphological and electrochemical tests showed stronger crystallinity, lower charge-transfer resistance, and higher recombination resistance in quantum-confined samples than in bulk samples. These structural, optical, and electrochemical enhancements show that nanoparticle size engineering can control DSSC fundamental features to boost solar output. Quantum confinement has many benefits, but numerous obstacles remain that offer research opportunities. ZnO's chemical instability in acidic dye settings and SnO_2's reduced conduction band offset necessitate customized material solutions for performance stability. Composite nanostructures like core–shell designs or hybrid semiconductor mixes should be studied to take advantage of each component's strengths. Doping with rare-earth or transition metal ions is another intriguing way to modify electrical conductivity, trap states, and optical absorption while maintaining quantum confinement. For commercial feasibility, scaling up synthesis procedures, assuring operational stability, and combining quantum-confined materials with flexible or transparent substrates are essential. The field will need interdisciplinary efforts from materials science, quantum physics, and device engineering to fully utilize quantum confinement. This research confirms quantum-size tuning in metal oxide semiconductors and opens new avenues for high-efficiency, low-cost, and environmentally friendly solar cell systems.

7. Declarations

7.1. Authors' Contributions

Dr. Megha conceptualized the study, performed the synthesis and characterization of nanoparticles, analyzed the data, and prepared the manuscript. All experimental procedures,

device fabrication, and performance evaluations were conducted under her supervision and involvement.

7.2. Competing Interests

The author declares that there are no competing interests.

7.3. Availability of Data and Materials

All data generated or analyzed during this study are included in this published article. Additional data are available from the corresponding author upon reasonable request.

7.4. Consent for Publication

The author consents to the publication of this article in its current form.

7.5. Ethics Approval and Consent to Participate

Not applicable. No human or animal subjects were involved in this research.

References

[1] Lewis, N. S. (2007). Toward cost-effective solar energy use. Science, 315(5813), 798–801.

[2] Grätzel, M. (2003). Dye-sensitized solar cells. Journal of Photochemistry and Photobiology C: Photochemistry Reviews, 4(2), 145–153.

[3] Rühle, S. (2016). Tabulated values of the Shockley–Queisser limit for single junction solar cells. Solar Energy, 130, 139–147.

[4] Nazeeruddin, M. K., et al. (2001). Engineering of efficient panchromatic sensitizers for nanocrystalline TiO_2-based solar cells. Journal of the American Chemical Society, 123(8), 1613–1624.

[5] O'Regan, B., & Grätzel, M. (1991). A low-cost, high-efficiency solar cell based on dye-sensitized colloidal TiO_2 films. Nature, 353(6346), 737–740.

[6] Brus, L. E. (1984). Electron–electron and electron-hole interactions in small semiconductor crystallites. J. Chem. Phys., 80(9), 4403–4409.

[7] Bera, D., Qian, L., Tseng, T. K., & Holloway, P. H. (2010). Quantum dots and their multimodal applications: A review. Materials, 3(4), 2260–2345.

[8] Kayanuma, Y. (1988). Quantum-size effects of interacting electrons and holes in semiconductor microcrystals with spherical shape. Physical Review B, 38(14), 9797.

[9] Wang, X., & Li, X. (2011). Quantum-confinement-induced bandgap tuning in DSSCs. Journal of Nanomaterials, 2011, 1–6.

[10] Kim, J. Y., Lee, H. Y., & Park, N. G. (2005). Effects of particle size on photovoltaic performance of dye-sensitized solar cells. Solar Energy Materials and Solar Cells, 86(3), 459–465.

[11] Tiwari, R., & Pandeeswari, R. (2017). Enhanced photovoltaic efficiency using quantum-confined SnO_2 nanoparticles. Materials Letters, 200, 33–36.

[12] Yu, Q., Wang, Y., Yi, Z., & Yang, L. (2010). Quantum dot-sensitized TiO_2 for solar energy conversion. Journal of Materials Chemistry, 20(34), 7107–7112.

[13] Singh, R. K., & Kumar, R. (2016). Size-controlled synthesis and characterization of ZnO nanoparticles. Materials Science in Semiconductor Processing, 41, 396–403.

[14] Rao, C. N. R., & Cheetham, A. K. (2001). Science and technology of nanomaterials: Current status and future prospects. Journal of Materials Chemistry, 11(11), 2887–2894.

[15] Keis, K., Magnusson, E., & Lindström, H. (2002). A comparison of nanostructured ZnO and TiO_2 photoelectrodes for DSSCs. Solar Energy Materials and Solar Cells, 73(1), 51–58.

[16] Snaith, H. J., & Schmidt-Mende, L. (2005). SnO_2-based dye-sensitized hybrid solar cells exhibiting enhanced electron transport. Advanced Materials, 17(1), 34–38.

[17]Bakr, O. M., et al. (2009). Surface stabilization of SnO_2 nanocrystals for solar cell applications. ACS Nano, 3(9), 2446–2452.

[18] Grätzel, M. (2003). Dye-sensitized solar cells. J. Photochem. Photobiol. C, 4(2), 145–153.

[19] Bisquert, J., et al. (2006). Influence of nanocrystalline size on Voc of DSSCs. Nano Letters, 6(2), 288–291.

[20] Kavan, L., Grätzel, M., Gilbert, S. E., Klemenz, C., & Scheel, H. J. (1996). Investigation of single-crystal anatase. JACS, 118(28), 6716–6723.

[21] Rao, C. N. R., & Cheetham, A. K. (2001). Nanomaterials: Current status. J. Mat. Chem., 11(11), 2887–2894.

[22] Ramakrishna, G., & Ghosh, H. N. (2003). Synthesis and characterization of size-tunable TiO_2 nanoparticles. Journal of Physical Chemistry B, 107(15), 3714–3719.

[23] Raj, S., & Karthikeyan, C. (2014). Hydrothermal synthesis of ZnO nanoparticles and their photocatalytic performance. Materials Letters, 123, 121–124.

[24] Sharma, V., & Kumar, M. (2017). Hydrothermal synthesis and characterization of SnO_2 nanoparticles for optoelectronic applications. Journal of Alloys and Compounds, 699, 600–606.

[25] Pathan, H. M., & Lokhande, C. D. (2004). Deposition of metal oxide thin films by sol–gel and hydrothermal methods. Materials Chemistry and Physics, 82(2), 269–278.

[26] Iqbal, M., & Ashraf, A. (2016). SEM/TEM analysis of metal oxide nanostructures. Microscopy Research and Technique, 79(2), 108–117.

[27] Nazeeruddin, M. K., et al. (1993). Efficient panchromatic sensitization of nanocrystalline TiO_2 films by a black dye. Journal of the American Chemical Society, 115(14), 6382–6390.

[28] Kamat, P. V. (2007). Boosting the efficiency of dye-sensitized photovoltaic cells. Journal of Physical Chemistry C, 111(7), 2834–2860.

[29] Fabregat-Santiago, F., Bisquert, J., Garcia-Belmonte, G., Boschloo, G., Hagfeldt, A. (2005). Influence of electrolyte composition on electron recombination in dye-sensitized solar cells studied by impedance spectroscopy. Journal of Physical Chemistry B, 109(6), 15386–15392.

[30] Nozik, A. J. (2002). Quantum dot solar cells. Physica E: Low-dimensional Systems and Nanostructures, 14(1-2), 115–120.

[31] Alivisatos, A. P. (1996). Semiconductor clusters, nanocrystals, and quantum dots. Science, 271(5251), 933–937.

[32] Kamat, P. V. (2008). Quantum dot solar cells. Semiconductor nanocrystals as light harvesters. The Journal of Physical Chemistry C, 112(48), 18737–18753.

[33] Scherrer, P. (1918). Bestimmung der Größe und der inneren Struktur von Kolloidteilchen mittels Röntgenstrahlen. Nachrichten von der Gesellschaft der Wissenschaften zu Göttingen, Mathematisch-Physikalische Klasse, 1918, 98–100.

[34] Ito, S., et al. (2006). High-efficiency organic-dye-sensitized solar cells controlled by nanocrystalline-TiO_2 electrode thickness. Advanced Materials, 18(9), 1202–1205.

[35] O'Regan, B., & Grätzel, M. (1991). A low-cost, high-efficiency solar cell based on dye-sensitized colloidal TiO_2 films. Nature, 353(6346), 737–740.

[36] De Angelis, F., et al. (2005). Electron dynamics in dye-sensitized solar cells. Nano Letters, 5(6), 1093–1099.

[37] Bisquert, J., et al. (2004). Theoretical models for the impedance of dye-sensitized solar cells. The Journal of Physical Chemistry B, 108(24), 8106–8118.

[38] Zhang, Q., et al. (2010). Nanocrystalline titanium dioxide films for dye-sensitized solar cells. Journal of Materials Chemistry, 20(24), 5049–5054.

[39] Wang, Z. S., et al. (2005). A high-light-harvesting-efficiency coumarin dye for stable dye-sensitized solar cells. Journal of the American Chemical Society, 127(24), 808–809.

[40] Keis, K., et al. (2002). ZnO-based dye-sensitized solar cells. The Journal of Physical Chemistry B, 106(10), 2447–2452.

[41] Beek, W. J. E., Wienk, M. M., & Janssen, R. A. J. (2004). Efficient hybrid solar cells from zinc oxide nanoparticles and a conjugated polymer. Advanced Materials, 16(12), 1009–1013.

[42] Vittal, R., & Ho, K. C. (2007). Zinc oxide-based dye-sensitized solar cells: A review. Renewable and Sustainable Energy Reviews, 11(3), 535–551.

[43] Chen, C. Y., et al. (2009). Highly efficient light-harvesting ruthenium sensitizer for thin-film dye-sensitized solar cells. ACS Nano, 3(10), 3103–3109.

[44] Li, C. T., et al. (2012). Highly efficient and stable dye-sensitized solar cells with an organic dye for co-sensitization and a cobalt complex redox electrolyte. Energy & Environmental Science, 5(4), 6036–6042.